TOXICOLOGICAL SCIENCES **113(1)**, 226–242 (2010)
doi:10.1093/toxsci/kfp247
Advance Access publication October 12, 2009

Subchronic 13-Week Inhalation Exposure of Rats to Multiwalled Carbon Nanotubes: Toxic Effects Are Determined by Density of Agglomerate Structures, Not Fibrillar Structures

Jürgen Pauluhn[1]

Department of Inhalation Toxicology, Institute of Toxicology, Bayer Schering Pharma, Building Number 514, 42096 Wuppertal, Germany

[1]For correspondence via fax: +49 (202) 364589. E-mail: juergen.pauluhn@bayerhealthcare.com.

Received July 21, 2009; accepted October 6, 2009

Wistar rats were nose-only exposed to multiwalled carbon nanotubes (MWCNT, Baytubes) in a subchronic 13-week inhalation study. The focus of study was on respiratory tract and systemic toxicity, including analysis of MWCNT biokinetics in the lungs and lung-associated lymph nodes (LALNs). The time course and concentration dependence of pulmonary effects were examined by bronchoalveolar lavage (BAL) and histopathology up to 6 months postexposure. Particular emphasis was directed to the comparative characterization of MWCNT structures prior to and after micronization and dry powder dispersion into inhalation chambers. These determinations were complemented by additional analyses in digested BAL cells. Animals were exposed on 6 h/day, 5 days per week for 13 consecutive weeks to 0, 0.1, 0.4, 1.5, and 6 mg/m^3. The subchronic exposure to respirable solid aerosols of MWCNT was tolerated without effects suggestive of systemic toxicity. Kinetic analyses demonstrated a markedly delayed clearance of MWCNT from lungs at overload conditions. Translocation into LALNs occurred at 1.5 and 6 mg/m^3 and required at least 13 weeks of study to become detectable. At these exposure levels, the lung and LALN weights were significantly increased. Sustained elevations in BAL polymorphonuclear neutrophils and soluble collagen occurred at these concentrations with borderline effects at 0.4 mg/m^3. Histopathology revealed principal exposure-related lesions at 0.4 mg/m^3 and above in the upper respiratory tract (goblet cell hyper- and/or metaplasia, eosinophilic globules, and focal turbinate remodeling) and the lower respiratory tract (inflammatory changes in the bronchioloalveolar region and increased interstitial collagen staining). Granulomatous changes and a time-dependent increase of a bronchioloalveolar hyperplasia occurred at 6 mg/m^3. All end points examined were unremarkable at 0.1 mg/m^3 (no-observed-adverse-effect-level). In summary, this study demonstrates that the induced pathological changes are consistent with overload-related phenomena. Hence, the etiopathological sequence of inflammatory events caused by this type of MWCNT appears to be related to the high displacement volume of the low-density MWCNT assemblage structure rather than to any yet ill-defined intrinsic toxic property. Thus, the hypothesis of study is verified, namely, common denominators between carbon black and MWCNT do exist.

Key Words: **nanoparticles; multiwalled carbon nanotubes; repeated inhalation exposure; disposition; respirability; clearance; aggregates; pulmonary and extrapulmonary toxicity; volume displacement overload.**

Carbon nanotubes (CNT) are novel materials attractive for use in many technical applications. Numerous studies have been performed to unravel their characteristic physical and electromechanical properties (Zbib *et al*., 2008). CNT have been reported to elicit toxic responses, ascribed so far to metal (catalyst) contamination, CNT length and aspect ratio, functionalization, degree of oxidation, defects, surface activity, and hydrophobicity (Fenoglio *et al*., 2008; Muller *et al*., 2008). *In vivo* toxicity studies of multiwalled CNTs (MWCNT) and especially inhalation toxicity studies are very limited. The results of these studies provide inconsistent evidence on the kind and degree of pulmonary and extrapulmonary toxicity (Shvedova *et al*., 2009). To a major extent, this lack of consistency appears to stem from the fact that multiple approaches have been used to make stable, liquid suspensions of MWCNT, whereas vehicle-free dry powder dispersions have received only limited attention (Baron *et al*., 2008). Likewise, an in depth characterization of MWCNT is complex, and, apart from mass, a unifying denominator characterizing the critical ''cumulative exposure dose'' has yet not been established. So far, these materials have been characterized prior to study; however, little appreciation has been given to quantify the form present following micronization and processing to make this hydrophobic material amenable to testing in biological systems (Warheit, 2008). Similarly, test-tube characterization cannot substitute the MWCNT characterization at target organ level or the site of initial deposition, which, potentially, is the entire respiratory tract (Pauluhn, 2009a).

Multiple studies (most of them by noninhalation routes) have contributed to the controversy surrounding the *in vivo* toxicity of MWCNT. However, state-of-the-art subchronic inhalation

bioassays according to internationally recognized and harmonized test protocols (Organisation for Co-Operation and Development [OECD]-GD#39, OECD, 2009; OECD#413, OECD, 2008) or published reference studies with carbonaceous or other poorly soluble particles (Bermudez *et al*., 2002, 2004; Elder *et al*., 2005) are scarce. The potential hazards ascribed to MWCNT have been detailed elsewhere, and any repetition is beyond the scope of this paper (Baron *et al*., 2008; Duffin *et al*., 2007; Oberdörster, 2002; Oberdörster *et al*., 2005, 2007; Shvedova *et al*., 2009; Warheit *et al*., 2004). Several intra-abdominal injection studies in mice using long and rigid-type MWCNT have received a great deal of attention because of their potential to induce extensive pleural inflammation and/or mesothelioma (Poland *et al*., 2008; Takagi *et al*., 2008). In a more recent intra-abdominal injection study with chronic postinstillation observation period, mesothelioma following injection of asbestos were produced but not with MWCNT (Muller *et al*., 2009). Experimental variables were considered to account for different outcomes.

The degree and kind of aggregation of MWCNT structures is determined by the rigidity of nanotubes and whether their diameters are thin enough to allow their buckling and self-aggregation into low-density, particle-like, intertwined, and coiled assemblages. Also the production method may impact the type of assemblage structure and whether it is stabilized by mere agglomeration or some kind of intertubular aggregation (physical entanglement). Hence, depending on these characteristics, agglomerate structures of nanotubes may differ appreciably from thin-walled MWCNT to thick-walled, rigid MWCNT. It is important to understand the resultant toxicological properties of these types of MWCNT and whether the critical toxicity arises from the individual tube structure (e.g., fiber) or the collective behavior of inhalable assemblages of nanotubes. Suffice it to say, the structure tested in any bioassay should resemble those potentially inhaled by humans under real-life exposure conditions while observing the particle size criteria called for by harmonized OECD testing guidelines.

This study focuses on the toxicological characterization of thin-walled MWCNT (Baytubes) in rats, a species recommended by current testing guidelines (OECD#413, OECD 2008). The MWCNT examined have a strong tendency to aggregate into microscopic bundles (assemblages), which in turn agglomerate loosely into small clumps that are mostly nonrespirable (see Fig. 1). This appears to be a common feature of CNT (Lam *et al*., 2006). The lack of using appropriate measures to reduce the size of clumps in injection/instillation studies may cause substantial artifacts (Pauluhn, 2009a). Therefore, to make these clumps respirable, the test substance was micronized to the extent to increase the dustiness of particles without affecting the structure of assemblages to any appreciable extent. Taking into account the postulated mechanisms and pathways through which MWCNT may induce their unexpected course of pulmonary response (Shvedova *et al*., 2009), four aspects were given particular attention: first, whether the shape and assemblage structures of nanotubes in exposure atmospheres and recovered from digested BAL cells of subchronically exposed rats differ; second, whether the cumulative target tissue dose of retained MWCNT correlates with the pulmonary inflammatory response over a postexposure period of 6 months; and third, whether these findings can be related to any volumetric inhibition of clearance of overloaded alveolar macrophages (International Life Science Institute, ILSI, 2000). The fourth objective was to verify/refute the hypothesis whether the lower mass concentrations of MWCNT required to attain volumetric overload are a unifying denominator of bridging results from carbon black (CB) (Elder *et al*., 2005) to MWCNT.

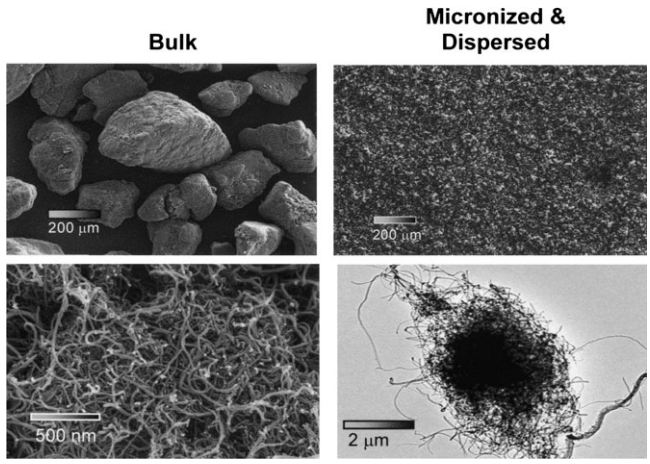

FIG. 1. Comparison of SEM images for bulk (left column) and micronized and dispersed (right column) Baytubes at different magnifications. Following dispersion into inhalation chambers, the airborne material was collected onto Nucleopore polycarbonate hydrophilic filters supported by a glass fiber filter.

MATERIALS AND METHODS

Test Material

The MWCNT addressed in this study are a proprietary product (Baytubes) of Bayer MaterialScience, Leverkusen, Germany. The physical characteristics of this material are summarized in Table 1. These MWCNT have a tendency to form coiled, intertwined, and tangled structures as depicted in Figures 1 and 2. They are characterized by a thin and relative narrow diameter in the range of 10 nm (Fig. 3). Length measurements of dispersed MWCNT in liquids by rigorous ultrasonication and subsequent characterization by transmission electron microscopy (TEM) demonstrated median tube lengths of pristine MWCNT in the range of 200–300 nm (Fig. 3). During the progression of study, several measurements with slightly varying sample preparation were made (data not shown). It is of note that some of them resulted in higher length medians (≈1000 nm). It appears as if the interpretation of measurements of the lengths of rigorously dispersed MWCNT bundles into single tubes must be tempered with caution because somewhat destructive conditions are required for sample preparation and analysis.

The physical properties of the test material and its low dustiness make inhalation testing experimentally demanding. Micronization was applied to increase the dustiness of the test material without destroying the assemblage structure of MWCNT. For micronization, a Retsch Centrifugal Ball Mill S100

TABLE 1
Characteristics of Test Substance

Baytubes	Bulk	Micronized	Inhalation chamber
Appearance of test material	Figure 1	Figure 1	Figure 2
Content of cobalt (Co) (%, wt/wt)—ICP-OES[a]	0.46	0.46	0.38
Content of cobalt (Co) (%, wt/wt)—AAS[b]	0.53	0.53	—
Elemental analysis (% carbon-oxygen)[c]	98.6–1.4	99.1–0.8	—
N_2-BET surface area (m^2/g)[d]	253	257	259
Bulk density (g/cm^3)[e]	0.16	0.11	—
Bulk by mercury pycnometry density (g/cm^3)[f]	0.32	0.31	—

[a]Inductive Coupled Plasma-Optical Emission Spectroscopy (ICP-OES) (Spectroflame, Spectro Analytical Instruments, Kleve, Germany).

[b]Atomic Absorption Spectroscopy-Graphite Furnace (AAS) (for details see tissue digestion method).

[c]ESCALab 220 XL, Thermo Fisher Scientific, Waltham, MA.

[d]Gemini 2360 (Micromeritics, Norcross, GA).

[e]Measurement analog to DIN/ISO 9136.

[f]Measurement analog to DIN 66133/ISO 15901-1. This method was used to measure the agglomerate density by mercury displacement pycnometry (for details, see Klobes *et al*., 2006).

(http://www.retsch.com/dltmp/www/808b12c73a43c42cdfd57224c6296b12/brochure_ball_mills_en.pdf) was used.

Animals

Specific pathogen-free, young adult male and female Wistar rats of the strain HsdCpb:WU (specified pathogen free) were purchased from Winkelmann, Borchen, Germany. At the commencement of the study, the rats were 2 months old and were acclimatized for approximately 2 weeks prior to the beginning of study. Animals were identified by individual transponders (Implantable Micro Identification [IMI] 1000, Biomedic Data Systems, BMDS, Seaford, DE), animal color marks, and cage labels. The transponders were subcutaneously (flank) injected after randomization using the IMI injection equipment. On each exposure day, the correct animal location in the respective chamber was verified using a digital reader (DAS 5002, BMDS). Rats were singly housed in polycarbonate cages containing low dust wood shavings as bedding material. A standard fixed-formula diet (KLIBA 3883 pellet maintenance diet for rats and mice; PROVIMI KLIBA SA, 4303 Kaiseraugst, Switzerland) and municipality tap water (drinking bottles) were available *ad libitum*. Housing conditions were in accordance to the European Union animal welfare regulations (European Community, Directive 86/609/EEC, 1986) with 12-h light/dark cycles. Temperature and relative humidity of animal holding rooms were in the range of 22°C and 40–60%, respectively.

Pilot Studies

The pulmonary toxicity, disposition, and impact of residual concentrations of cobalt (Co) in this MWCNT were examined in rats using a single 6-h nose-only inhalation (11 and 241 mg/m^3) followed by a maximum postexposure period of 3 months (Pauluhn, 2009a; Ellinger and Pauluhn, 2010). The results of this pre-study had the following impact on the study design used in this study: (1) pulmonary toxicity appears to be driven by assemblage structure, not the residual content of Co, and (2) the analytically verified content of matrix-bound Co is 0.115% while the balance to 0.53% is surface bound and potentially leachable Co. Therefore, for dosimetric calculations of lung burdens, only the former percentage was considered.

Study Design

Subchronic inhalation study. Exposure concentrations were selected based on published evidence with the carbonaceous material CB (Elder *et al*., 2005). In that study, a significant increase of BAL polymorphonuclear neutrophil (PMN) did not occur in rats following a 13-week exposure to 1 mg/m^3 CB. Particle clearance was prolonged (1, 7, and 50 mg/m^3: $t_{1/2} = 107$, 329, and 667 days, respectively; recalculation and personal communication by A. Elder). Due to the low specific density of Baytube agglomerates (≈0.1–0.3 g/cm^3) relative to CB (≈1.8 g/cm^3), the displacement volumes of the MWCNT assemblages with similar aerodynamic properties may differ appreciably (approximately up to an order of magnitude, Pauluhn, 2009a). Any better estimation is subject to errors as the specific density of CB may not have been determined using the same methodology as used for this MWCNT (see legend of Table 1). Conceptually, this approach assumes that agglomerates are present as spherical assemblages of intertwined tubes. This has been verified by image analysis from air samples (Fig. 1); however, assemblage structures were variable and also deviated from this idealized spherical structure and had somewhat frayed surfaces (Fig. 2). Based on the rationale detailed above, this means that MWCNT should be approximately 10 times more potent than CB due to their higher displacement volume in alveolar macrophages (see ILSI, 2000) and 0.1, 0.4, 1.5, and 6 mg/m^3 were selected as target concentrations. Based on this hypothesis, 0.1 mg/m^3 is estimated to be in the nonoverload range and 0.4 mg/m^3 is assumed to be at that transitional level at which lung overload may occur. Frank lung overload with partial or inhibited clearance is anticipated to occur at 1.5 and 6 mg/m^3.

At the end of the acclimatization period, the rats were randomly assigned to five exposure groups of 50 male rats per group and 10 female rats per group each of which was exposed by nose only for 13 weeks (6 h/day on 5 days/week). Satellite groups (male rats only) were examined during a postexposure period of maximal 6 months. Pulmonary toxicity was characterized by histopathology (right lung lobes, lavaged) and BAL during weeks 8 (interim sacrifice), 13 (end of exposure period), 17, 26, and 39 (exposure commenced in week 0). Pulmonary dosimetry (left lung lobe) and translocation of the

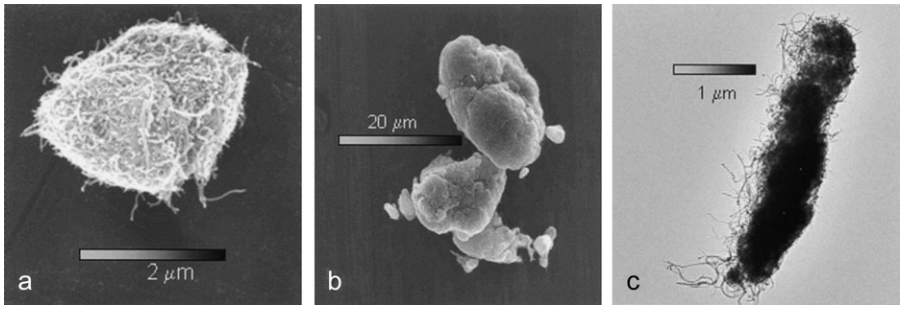

FIG. 2. Image analysis by SEM of Baytubes dispersed into inhalation chambers. (a) Morphology of MWCNT agglomerate collected on an impaction plate of a critical orifice cascade impactor, (b) MWCNT agglomerates collected on the cascade impactor stage 8–16 µm, and (c) TEM image of Baytubes collected directly into TEM grids.

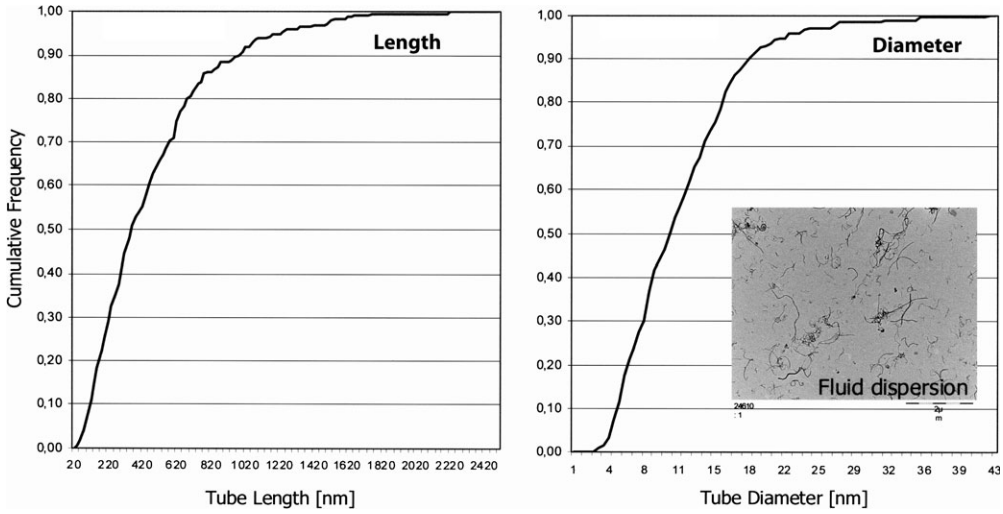

FIG. 3. Measurements of the lengths/diameter frequency distributions of isolated fibrillar structures from rigorously dispersed Baytubes (ultrasonication in ethanol for 5 min at room temperature, 35 kHz) and subsequent characterization by TEM. Approximately 200–300 tubes were counted (size bar in offset: 2 μm).

tracer Co to the lung-associated lymph nodes (LALNs) were determined at the same time points in six male rats per group per time point. All main group animals (10 rats per group per sex) were examined in week 13 as detailed below.

Clinical observations were systematically performed on individual rats before and after each exposure. Body weights were recorded twice weekly on Mondays and Fridays during the exposure period and once weekly during the postexposure period. During the exposure period, food and water consumption were determined once per week. Rectal temperatures and reflexes were repetitively determined during the exposure period (after exposure). Ophthalmology was performed prior to start and at the end of the exposure period. At the terminal sacrifice (week 13), following gross pathological examination of rats, organ weights (adrenal glands, brain, heart, kidneys, liver, lung, LALNs, ovaries, spleen, testes, and thymus) were determined. After fixation and preservation (10% neutral-buffered formalin with the exception of optic nerve and testes which were fixed in Davidson's solution), the following organs from main group rats of all exposure groups were fixed and examined by light microscopy (entire respiratory tract and LALN: all groups; extrapulmonary organs: control and high group): adrenals, aorta, bone (femur), including joint and bone marrow (in femur and sternum and bone marrow smear), brain (cerebrum, cerebellum, and "medulla oblongata"), coagulating gland, epididymides (including accessory glands), esophagus, eyes (including eyelids), harderian gland, head (pharynx and nasal cavities according to Young, 1981), heart, stomach, duodenum, jejunum, ileum, cecum, colon, rectum, kidneys with pelvis, lachrymal glands (extraorbital glands), larynx, liver, lungs, lymph nodes (hilar region, cervical, mandibular, mesenteric, and poplitetal), mammary gland, muscles (biceps and quadriceps), ovaries, pancreas, parathyroids, pituitary, prostate, salivary glands (head), sciatic nerve, seminal vesicles, skin (flank and muzzle/facial area), spinal cord (cervical, thoracic, and lumbar), spleen, sternum, testes, thymus, thyroid, tongue, trachea, urinary bladder, ureters, urethra, uterus (including cervix), vagina, and zymbal glands.

General hematology, clinical pathology, and urinalysis were performed at the end of the 13-week study period on 10 rats per group per sex. The parameters determined were compliant with those defined by OECD#413 (OECD 2008). This study was conducted in compliance with the OECD Principles of Good Laboratory Practice as revised in 1997 (ENV/MC/CHEM(98)17) and with the revised German Principles of Good Laboratory Practice according to Annex I German Chemicals Act (Bundesgesetzblatt, Volume 2008, Part I, No 28, 1173–1184, issued 11 July 2008).

Inhalation Exposures to MWCNT

The micronized MWCNT were dispersed into inhalation chambers using a Wright-Dust-Feeder (BGI Inc., Waltham, MA). For dry powder dispersion (160–180 kPa), compressed dry air was used. Prior to entering the nose-only inhalation chamber, a cyclone and pull/push dilution system were used to achieve the targeted particle size and concentration. The flow rate per exposure port was 0.75 l/min. The inhalation chamber system used had 80 exposure ports in total. Under these test conditions, steady state is attained within 1 min of chamber operation. Airflows were monitored by calibrated (Bios DryCal Defender 510) mass flowmeters. Control of the inhalation chamber and management of all physical inhalation chamber data, including the current calibration data, were performed using a computerized and validated data acquisition and control system. Further details of this modular chamber and its validation have been published in detail elsewhere (Pauluhn, 1994, 2005, 2009b; Pauluhn and Thiel, 2007).

Exposure Atmosphere Characterization

The tolerance limits for diameters of probe orifices were calculated using published formulas to minimize anisokinetic sampling errors (Pauluhn, 1994; Willeke and Baron, 1993). The stability of the aerosol generation system was monitored using a Microdust Pro (Casella, Amherst, MA) digital real-time aerosol photometer. In addition, at 0.1 mg/m^3 only, a tapered element oscillating microbalance (TEOM) 1400a (Thermo Scientific, Environmental Instruments, Franklin, MA) system was used. Total mass concentration was determined by gravimetric analysis (filter: glass fiber filter, Sartorius, Göttingen, Germany). Particle size analyses utilized a low-pressure critical orifice Berner-type AERAS LPI 4/0.015/2 stainless steel cascade impactor (HAUKE, Gmunden, Austria). Silicon-coated aluminum foil served as collection medium of particles. The mass median aerodynamic diameter (MMAD) and the geometric SD were calculated as described previously (Pauluhn, 2005). Additional measurements were made using a TSI-Aerodynamic Particle Sizer (APS) 3321 with TSI Diluter 3302 (TSI Inc., Shoreview, MN). This device detects particles in the range of 0.5–20 μm. Additional samples were specifically collected for nanoparticle analyses (scanning mobility particle sizer [SMPS]/particle counting system [Grimm Aerosoltechnik GmbH, Ainring, Germany], Whatman polycarbonate filters, supported by Sartorius glass fiber filters, for TEM analyses). Active volumetric flow control is maintained by mass flow controllers whose set points are online adjusted in accordance with the measured ambient temperature and pressure. All samples were taken from the vicinity of the rats' breathing zone.

Measurement of Cellular and Biochemical End Points in BAL

Briefly, rats were anesthetized with sodium pentobarbital and completely exsanguinated by severing the "aorta abdominals." The excised wet lungs were weighed and, following ligation of the bronchus leading to the left lung, then the right lung lobes were then lavaged via a tracheal cannula with two volumes of 5 ml of physiological saline (at 37°C) and four lavage cycles in total. BAL was centrifuged at 200 × g for 10 min. Cytospots were prepared (2×10^5 per cytospot) and differentiated by light microscopy (300 cells were counted per cytospot). The following end points were determined in the supernatant: total cell count, alkaline phosphatase, soluble collagen, lactate dehydrogenase (LDH), total protein, γ-glutamyltransferase (γ-GT), and β-N-acetyl glucosaminidase (β-NAG). Soluble collagen was assayed using the Sircol kit (http://www.biocolor.co.uk/sircol.html). This assay uses Sirius red as chromophore to quantify collagen (same stain as used for histopathology). Further methodological details have been published elsewhere (Pauluhn, 2009b).

Tissue Processing for Respiratory Tract Histopathology

Examinations utilized both lavaged and nonlavaged lungs. It has been demonstrated that even 12 saline washings appeared to have a negligible effect on the histological appearance of the lung as viewed with the light microscope and that it was nearly impossible to distinguish between washed and unwashed lungs (Brain and Frank, 1968a,b). Nonlavaged whole lungs were examined at the week 13 sacrifice while lavaged lungs (right lobes) were examined at all other sacrifices. While the bronchus to the left lung lobe was tied up to allow lavage and instillation fixation of the right lung lobes, the left lobe was dissected and used for tracer determinations. Lungs were inflated at a pressure of approximately 20 cm H_2O with 10% neutral-buffered formalin and then fixed similarly by immersion. Histopathology was conducted on all preserved lung lobes, LALNs from the hilar region, and nasal passages, including sections of the ethmoid turbinates and the nerve axon transition to the brain and the olfactory bulb (week 13). The sectioning of the nasal passages and the larynx was consistent with the method published elsewhere (Kaufmann *et al*., 2009; Young, 1981). At all other sacrifices, the lung only was examined (all exposure levels). The head with nasal cavities was decalcified (citrate-formic acid) at room temperature for 3 weeks and then, similar to all other sections, embedded with paraplast. Slides were stained with hematoxylin & eosin. Lungs were additionally stained with Sirius red for the diagnosis of collagen.

Determination of Morphology of MWCNT in BAL Cells

Specimens were from rats exposed at 0 or 6 mg/m^3. This analysis focused on the cells harvested by BAL in weeks 13 and 39. Air-dried cell pellets from cytospin preparations were incubated with fresh 10–15% sodium hypochlorite solution (Sigma-Aldrich 42,504-4). A total of 40 µl was transferred onto a single-cell pellet. Extraction was allowed to proceed at room temperature for 10 min, and its progression was controlled by light microscopy. Inverted light microscopy revealed that by this procedure, the majority of dark inclusions could be retrieved in the collection fluid. The collected fluid was then incubated for 2 h at room temperature before particles were prepared for scanning electron microscope (SEM) analysis. Frequency distributions of particles were concentrated onto a spot of 3–4 mm in diameter. The content of Co in air-dried cells (without digestion) or retrieved particle structures was analyzed after coating with carbon and SEM-Energy Dispersive X-ray (EDX) analysis (field emission SEM, Zeiss DSM982, operated at 15.0 kV). Element Analysis was carried out with Noran Software. The size of retrieved structures utilized digital images (1024 × 1024 or 512 × 512 pixels) was analyzed by Program Image J (version 1.410, http://rsb.info.nih.gov/ij). The long axis of all particles with clearly visible contours was measured in relation to the scale bar generated by the SEM. Attempts to demonstrate Co in these assemblages by SEM-EDX failed due to their low content in MWCNT (limit of quantification ≈1% Co).

Determination of MWCNT Lung and LALN Burdens

Biological specimens (left lung lobe and LALNs) were collected for the determination of Co as marker of exposure during weeks 8, 13, 17, 26, and 39. Organ aliquots were digested and in inorganic acids and microwaved. For all analyses, blank solutions and a standard solution of Co were used (PerkinElmer AAnalyst 700 high-performance atomic absorption spectrometer [graphite mode]). Further methodological details have been published elsewhere (Pauluhn, 2009b).

Kinetic Analysis of Co Lung Burdens

Lung burdens were calculated utilizing the following equation of the daily dose of Co deposited in the alveolar region (AlvDepDose-Co_{day}):

$$\mathrm{AlvDepDose-Co_{day}} = \mathrm{conc.}\frac{\mathrm{ng}}{L} \times \mathrm{MV_{rat}}\frac{L}{\mathrm{day}} \times \mathrm{AlvDepFraction_{MPPD2}} \times \mathrm{cobalt}\frac{\%}{100} = \frac{\mathrm{ng\,Co}}{\mathrm{rat-day}}.$$

The concentration (conc.) was the average total mass concentration of MWCNT obtained by filter analyses (Table 2). The respiratory minute volume (MV) was 0.8 l/min/kg rat (this respiratory MV was determined under nose-only exposure conditions similar to this study; Mauderly, 1986; Pauluhn and Thiel, 2007). The fraction of MWCNT deposited in the pulmonary region (AlvDepFraction) was 5.7% (estimated by the MPPD2 software; Anjilvel and Asgharian, 1995; RIVM, 2002) using the particle size data from cascade impactor analyses (Table 2). The content of matrix-bound Co was considered for calculation (0.115%) as detailed elsewhere (Ellinger and Pauluhn, in preparation).

For simulation of the exposure-related accumulation of the matrix-bound Co in the lung, we utilized the following relationship: $dc/dt = a(1 - kt)$, where k is the first-order elimination constant empirically determined during the 6-month postexposure period (based on Co lung burdens determined during postexposure weeks 17, 26, and 39). The elimination halftime was calculated as follows: $t_{1/2} = \ln(2)/k$. The daily increment of particle dose deposited in the alveoli "a" is equal to the "AlvDepDose-Co_{day}." During exposure days, the fraction of the dose increment was added to each of the arrays, and the total accumulated lung dose was then calculated over the entire exposure period by superposition of the arrays. A Fortran computer code was used for calculations.

Data Analysis

Body weights, BAL data, organ weights, food and water consumption, hematology, clinical pathology, and urinalysis data were compared using one-way ANOVA and Dunnett or Tukey-Kramer *post hoc* tests. Histopathological findings were compared with the concurrent control using Fisher's Exact Test. For all tests, the criterion for statistical significance was set at $p < 0.05$. Asterisks in figures and tables denote statistically significant differences to the concurrent air control group, $*p < 0.05$ and $**p < 0.01$.

RESULTS

MWCNT Characterization

The dustiness and particle size of pristine Baytubes are inadequate for state-of-the-art subchronic inhalation testing in rats according to current testing guidelines (OECD#GD39, OECD 2009). Therefore, the test substance was subjected to short micronization to increase its dustiness, however, without deterioration of the typical agglomerate structure of these MWCNT. The Brunauer-Emmett-Teller nitrogen gas adsorption (N_2-BET) surface area (Brunauer *et al*., 1938) and the content of residual Co were not affected by micronization (Table 1). This comparison demonstrates that the physical

TABLE 2
Generation and Characterization of Chamber Atmospheres

	Baytubes				
Target concentration (mg/m^3)	0	0.1	0.4	1.5	6.0
Gravimetric concentration (mg/m^3)	—	0.10 ± 0.02 (n = 68)	0.45 ± 0.06 (n = 54)	1.62 ± 0.2 (n = 207)	5.98 ± 0.8 (n = 207)
Total chamber airflow (l/min)	60	60	60	60	60
Temperature chamber (°C)	22.0 ± 2.7	22.0 ± 2.7	21.9 ± 2.7	22.1 ± 0.4	22.9 ± 0.4
Relative humidity chamber (%)[a]	≤ 5	≤ 5	≤ 5	≤ 5	≤ 5
Critical orifice cascade impactor					
MMAD (μm)	—	—	3.05 ± 0.3 (n = 14)	2.74 ± 0.2 (n = 41)	3.42 ± 0.2 (n = 41)
GSD	—	—	1.98 ± 0.2	2.11 ± 0.1	2.14 ± 0.2
Respirability (% mass < 3 μm)	—	—	49.8 ± 5.1	55.0 ± 4.1	43.3 ± 3.5
Mass concentration (mg/m^3)	—	—	0.4 ± 0.0.05	1.53 ± 0.2	5.68 ± 0.8
TSI APS 3321					
MMAD (μm)	—	1.67 ± 0.1 (n = 15)	1.91 ± 0.11 (n = 15)	1.93 ± 0.09 (n = 15)	2.19 ± 0.13 (n = 15)
NMAD (μm)	—	0.90 ± 0.02	0.93 ± 0.02	0.93 ± 0.09	0.94 ± 0.02
GSD	—	1.70 ± 0.3	1.68 ± 0.09	1.67 ± 0.1	1.76 ± 0.3
Number concentration (#/cm^3)	—	8.07 ± 2.4	39.6 ± 11.5	165.9 ± 56.0	363.5 ± 108.8
SMPS-CMAD (n = 2)					
Range 11–1083 nm (#/cm^3)	5	75	320	908	1763
Range 11–92 nm (% of total)	40	57	65	65	70

Note. CMAD: count median aerodynamic diameter; GSD, geometric SD (Grimm Aerosoltechnik GmbH); —, not applicable.

[a]Lower confidence range of humidity sensor 5%. Values represent means ± SDs. Off-line sampling activities (n reflects the number of filter and particle analyses per group) that were adequately spaced during the course of the 13-week exposure period. Temperature and humidity values were continuously recorded online and means and SDs were from daily means. Airflow rates were electronically controlled and adjusted to the set flow rate.

characteristics of the pristine bulk and micronized dispersed MWCNT were essentially identical and that the applied procedures did not change the assemblage structure to any appreciable extent (Table 1). The prevailing structures in inhalation chambers were identified by image analysis as coiled, tangled assemblages of MWCNT (Figs. 1 and 2). Depending on the sampling medium chosen (filter samples, aluminum foil–covered stages from critical orifice cascade impactor, and TEM grids), the structure of assemblages ranged from densely coiled sphere-like without/with frayed surface to more bundled agglomerates of tubes (Fig. 2). Some structures showed loose ends of single MWCNT protruding from the assemblage (Fig. 1). Isolated fibrils or isometric solid particles were not found by any method.

The images from MWCNT dispersed into inhalation chambers demonstrate, apart from total mass and the mass-based aerodynamic diameter, that there is no simple, unifying metrics describing unequivocally the physical properties of such complex test material. Collectively, the agglomerated structures appear to resemble low-density spheres of packed, tangled, and intertwined MWCNT. Pulmonary deposition cannot readily be estimated for such types of structures for two reasons: (1) for such low-density structures (see Table 1), the geometric diameter becomes appreciably larger than the aerodynamic diameter and (2) "loose ends" of individual tubes might favor deposition by interceptive forces in addition to the common inertia forces.

Measurements from exposure atmospheres were complemented by measurements of MWCNT structures retained in digested alveolar macrophages. The agglomerated material found in control rats was free of breakage products from fibrillar/tubular fibers. The lead structure of MWCNT found in alveolar macrophages was identical to that found in air (Figs. 2 and 4). The frequency distribution of agglomerated particle structures in digested BAL cells depicted in Figure 4 delineates a median geometric assemblage diameter in the range of 2–3 μm independent of the elapsed postexposure time.

Exposure Atmosphere Characterization

The aerosol size distribution from the rats' breathing zone samples utilized both a critical orifice Berner-type cascade impactor and a TSI APS 3321 laser velocimeter. Despite entirely different physical principles, both methods demonstrated fairly identical results (Table 2, Fig. 5). The total mass concentrations collected by the cascade impactor were identical to filter analyses (Table 2). This identical mass balance demonstrates that anisokinetic sampling errors or specific particle losses within the cascade impactor did not occur to any appreciable extent. Although the results from SMPS count analyses are difficult to put into any "mass-based" perspective, these measurements show that even under conditions of rigorous dispersion the number concentration of nanoparticles is minimal. The count mode was in the range of 35 nm (Table 2, Fig. 5, lower panel).

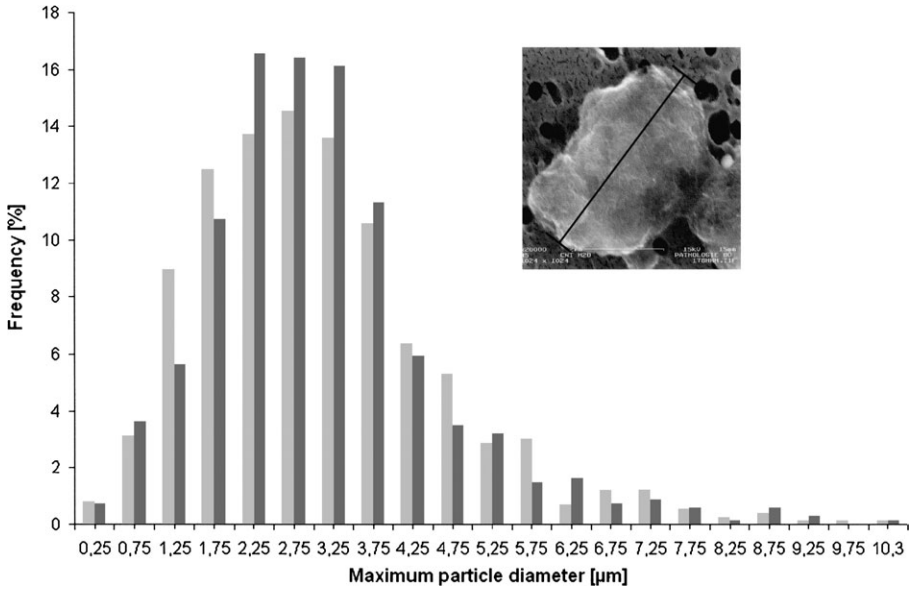

FIG. 4. Frequency distribution of the maximum MWCNT assemblage diameter (see inset) isolated from digested BAL cells. Light gray columns: lung lavage at the end of the 13-week exposure period (737 structures counted), dark columns: BAL cell collected at the end of the 6-month postexposure period (690 structures counted). Specimens were from rats exposed at 6 mg/m^3.

Observations, Body Weights, Food/Water Consumption, and Ophthalmology

The 13-week exposure to MWCNT was tolerated without substance-induced clinical signs of toxicity, mortality, changes in reflexes, changes in body temperature, body weights, and food and water consumption. Ophthalmology did not reveal any specific findings (data not shown). At 0, 0.1, 0.4, 1.5, and 6 mg/m^3, the body weights (means ± SDs) were at the commencement of study (day 0) as follows (males, 40 rats per group): 231 ± 9.9, 226 ± 9.8, 227 ± 9.9, 227 ± 9.0, and 228 ± 9.6 g, respectively; females (10 rats per group): 183 ± 5.6, 178 ± 6.6, 177 ± 8.1, 179 ± 9.3, and 180 ± 7.0 g, respectively. At the end of the 13-week exposure period, the respective body weights of male rats were 369 ± 23.6, 341 ± 29.5, 356 ± 26.6, 356 ± 27.1, and 356 ± 30.1 g; females: 245 ± 10.9, 227 ± 12.8, 225 ± 17.9, 231 ± 13.7, and 232 ± 13.7 g.

Clinical Pathology, Hematology, and Urinalysis

Data of rats from the MWCNT exposure were within the variability of the time-matched concurrent control group. All parameters evaluated, including blood leukocyte counts and differentials, were indistinguishable among the exposure groups (data not shown).

MWCNT Disposition in Lungs and LALNs

The time-course analyses of Co lung and LALN burdens are delineated in Figures 6 and 7, respectively. Kinetic time-course analyses yielded elimination halftimes of $t_{1/2}$ = 151, 350, 318, and 375 days at 0.1, 0.4, 1.5, and 6 mg/m^3. At 0.1 mg/m^3, most measurements of Co in the lung were in the range of the limit of quantification, which precluded a precise determination of $t_{1/2}$ at this exposure level. The simulated cumulative lung burdens of Co matched reasonably well the empirical data (Fig. 6) and thus confirmed the parameterization used. While the increased cumulative lung burden was proportional to the exposure concentration, an exposure duration–related increase was not apparent during exposure weeks 8–13. A clearly time- and concentration-dependent increase of Co into the hilus lymph nodes (LALNs) occurred at 1.5 and 6 mg/m^3 during the postexposure period (Fig. 7).

Bronchoalveolar Lavage

A summary of cellular and biochemical measurements in BAL is presented in Figures 8 and 9, respectively. To allow a better comparison of these end points, all biochemical end points were normalized relative to the time-matched, concurrent control group (= 100%). The cytodifferentiation of BAL cells was hampered due to the black pigmentation of MWCNT-laden BAL cells and their transition to lysis as well as variable stages of apparent cellular necrosis/apoptosis. Macrophages with ''vacuolated or foamy appearance'' were increased at 1.5 mg/m^3 and above. At these exposure concentrations, total cell counts and lymphocytes were increased at all time points. Neutrophilic granulocytes (PMNs), compared either as absolute counts or the percentage of cells in cytospins, were significantly increased at 0.4 mg/m^3 and above (Fig. 8). Based on the relative ranking of the parameters measured, the magnitude of changes were highest for PMNs and soluble collagen followed by LDH, γ-GT, total protein, β-NAG, and alkaline phosphatase (Figs. 8 and 9).

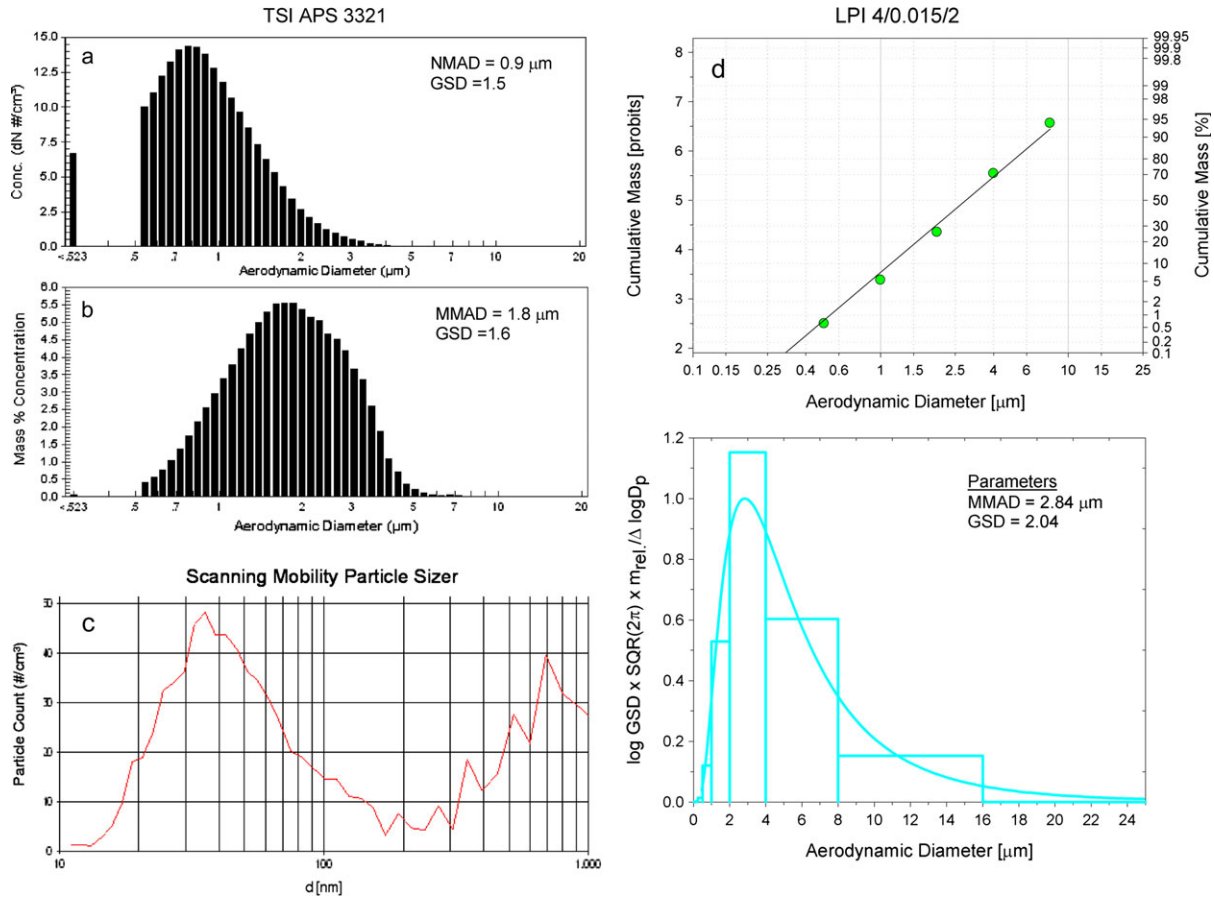

FIG. 5. Particle size analyses of Baytubes in inhalation chambers at 1.5 mg/m^3. TSI APS 3321 count (a) and mass (b) particle distributions in the range 0.5–20 mm, (c) count distributions of particles in the size range of 0.01–1 mm using an SMPS, and (d) mass distribution of particles using a critical orifice Berner-type cascade impactor LPI 4/0.015/2 with effective cutoff diameters in the range of 0.016–16 mm. Parameters were calculated from the cumulative mass distribution (upper panel). The normalized mass collected on the cascade impactor stages (bars) is compared with the mathematical curve fit (solid line) in the lower panel.

Except for γ-GT, all end points had in common that they increased from exposure weeks 8–13 followed by a decrease over time especially during the first postexposure month. Whereas changes stayed elevated at the high exposure concentrations (1.5 and 6 mg/m^3), a gradual decrease was apparent at lower exposure concentrations during the remaining postexposure period. While increases in soluble BAL-collagen correlated with BAL-protein and BAL-LDH (data not shown), the most consistent correlation existed for PMNs over a wide range (Fig. 10).

Organ Weights and Histopathology

With the exception of increased lung and LALN weights (Fig. 11), there were no other significant changes in organ weights, the organ-to-body weight, or the organ-to-brain weight ratios (data not shown). Significant increases occurred at 0.4 mg/m^3 and above. Exposure-related histopathology was present in the nasal passages, lung, and LALNs of rats exposed at 0.4 mg/m^3 and above. In the larynx, no differences to the control were observed. Slightly increased mucus and/or cells occurred in the pharynx and trachea of rats exposed at 1.5 and 6 mg/m^3 (data not shown). Sex-related differences were not apparent. In none of the additionally examined extrapulmonary tissues, MWCNT-induced changes were found.

At 1 day postexposure (week 13), the principal exposure-related lesions in the upper respiratory tract were characterized by goblet cell hyper- and/or metaplasia, eosinophilic globules, and focal turbinate remodeling (thickening of turbinate bone with increased activity of osteoblasts) at 1.5 and 6 mg/m^3. Eosinophilic globules or goblet cell hyper/metaplasia were already apparent in some rats exposed at 0.4 mg/m^3. There was no evidence of particle translocation to or reactive changes in the "bulbus olfactorius." Lesions surrounding the bronchioloalveolar region were characterized by thickening of epithelial cell layers and influx of inflammatory cells at 1.5 and especially 6 mg/m^3 with gradually less prominent changes at 0.4 mg/m^3. Slight to moderate inflammation, focally also with granulomatous appearance, was observed in rats exposed at 6 mg/m^3. At this exposure concentration, a time-dependent increase of a multifocal bronchioloalveolar hyperplasia was evident. The time course and concentration-dependence of the most salient lesions in the lung are summarized in Table 3. The comparison

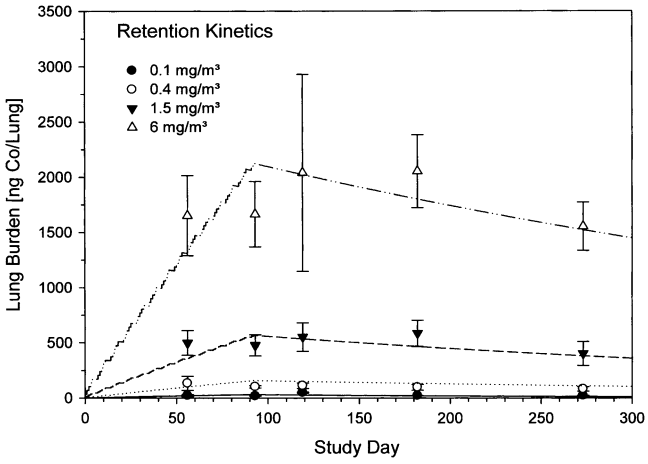

FIG. 6. Comparison of calculated and empirical concentrations of Co in the lungs of rats exposed for 13 weeks (6 h/day, 5 days/week). Data points represent the mean ± SD of six male rats examined on study weeks 13 (postexposure day 1), 17, 26, and 39.

of findings from lungs of rats sacrificed in week 13 (nonlavaged lungs) with all other sacrifices (lavaged lungs) did not reveal differences attributable to the lavage procedure (Table 3).

Increased interstitial collagen staining (Sirius red) occurred at 1.5 and 6 mg/m^3. Focal areas of increased collagen staining were adjacent to sites of increased particle deposition and inflammatory infiltrates (onset at 0.4 mg/m^3, see Table 3). Increased septal collagen staining was depicted as equal to interstitial fibrosis (for details, see Fig. 12). Thickening of the visceral pleura, due to an increased pleura space and more abundant Sirius red–stained tissue with/without inflammatory infiltrates and particle-laden macrophages, was noticed at 1.5 and 6 mg/m^3 (Table 3). Black pigmentation of LALNs, accompanied by increased paracortical cellularity, and increased bronchus-associated lymphoid tissue containing black particle-laden macrophages occurred at all particle exposure levels. These changes gained statistical significance at 0.4 mg/m^3 and above (data not shown). Collectively, pulmonary lesions were related to inflammatory responses at the site of initial deposition and retention of MWCNT structures at 1.5 and 6.0 mg/m^3. Minimal changes were already apparent at 0.4 mg/m^3.

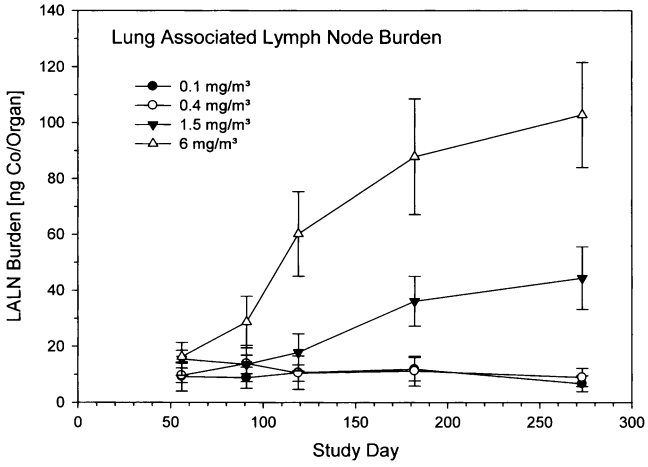

FIG. 7. Time course and concentration dependence of Co in LALNs from rats exposed for 13 weeks (6 h/day, 5 days/week). Data points represent the mean ± SD of six male rats examined on study weeks 13 (postexposure day 1), 17, 26, and 39.

DISCUSSION

Over the past 5 years, there has been a continuing debate on the most appropriate strategies to use for identifying and evaluating the human health risks of nanomaterials (Maynard, 2007; Walker and Bucher, 2009). One major prerequisite of this is to define a unifying metric of (target tissue) dose, which then serves as basis for the comparison of potencies of different substances. For MWCNT, particle size is among the most important physical properties as it affects, apart from the site, the cumulative dose deposited and retained within the lower respiratory tract. Conventional repeated inhalation toxicity testing uses highly standardized MMADs, preferentially in the range of 1–3 μm (OECD#GD39, OECD 2009; OECD#413, OECD 2008). Accordingly, hazards identified in such rat bioassays need to be put into a real-world human exposure perspective because humans may be encountered with smaller or more often larger particles than used in animal bioassays. Nonetheless, if interpreted thoughtfully, this standardized and inherently conservative rat inhalation bioassay generates invaluable data to derive risk guidance values for humans, for example, workplace limits, without the need of highly error-prone route-to-route or regimen-to-regimen extrapolations (Pauluhn, 2010). Micronization was applied to minimize the size of clumps but not the structure of MWCNT assemblages. Based on the hypothesis of study, the critical toxicity of MWCNT may not arise from the individual tube structure following mechanical destruction of the assemblage rather than from the collective behavior of nanotubes in inhalable assemblages as defined in Figures 1, 2, and 4. The empirical verification of what constitutes the most abundant MWCNT structure utilized analyses from inhalation atmospheres and digested BAL cells, which showed no differences of MWCNT structures from the starting material, the dispersed MWCNT into inhalation chamber atmospheres, and MWCNT deposited and retained in lung cells. Similar lead structures were also found by other authors using different micronization and/or dispersion principles (single-walled CNT: Baron *et al.*, 2008; MWCNT: Ma-Hock *et al.*, 2009). Future analyses following the downstream use of these types of MWCNT will verify/refute as to whether this lead structure is that prevailing in workplace atmospheres.

The focus of this subchronic inhalation study was to study this specific type of MWCNT using a range of exposure concentrations following the cornerstones of the National

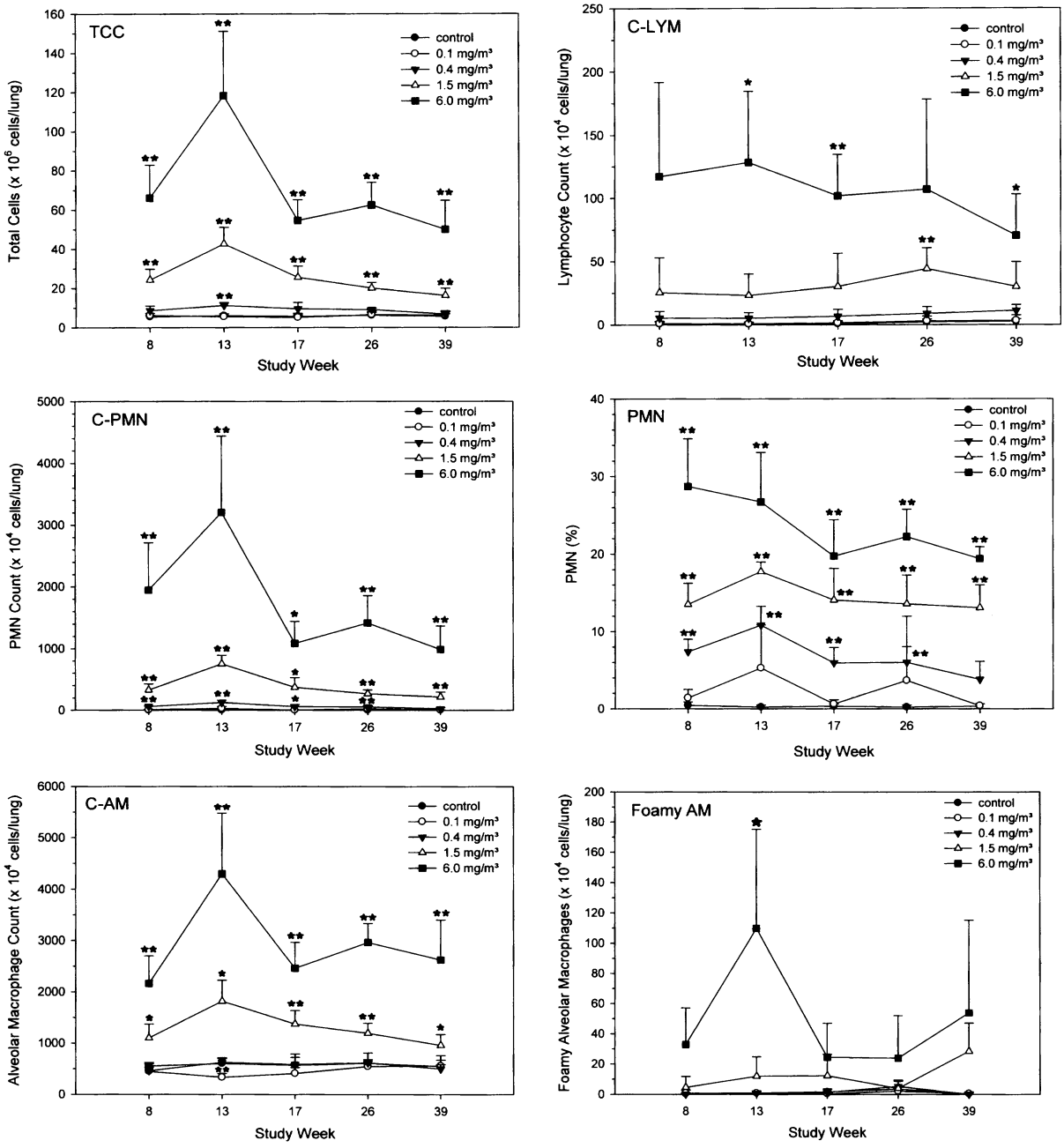

FIG. 8. Comparison of cellular inflammatory end points in BAL from rats exposed for 8 weeks (interim sacrifice) and 13 weeks (6 h/day, 5 days/week). Data points represent the mean ± SD of six male rats examined on study weeks 13 (postexposure day 1), 17, 26, and 39. Asterisks denote statistical significance to the time-matched control (*$p < 0.05$, **$p < 0.01$).

Research Council (NRC) paradigm (NRC, 2007). The concentrations of this study were selected based on the most comprehensive, recent subchronic inhalation study on rats with CB reported by Elder *et al.* (2005). However, the concentrations selected took into account the markedly different specific densities of CB and MWCNT assemblages. As detailed elsewhere (Pauluhn, 2009a), the lower agglomerate density of MWCNT relative to CB may be conducive to attain volumetric overload of alveolar macrophages (for a detailed discussion of particle-induced overload, see ILSI, 2000; Pauluhn, 2009a) at approximately 10-fold lower concentrations. Accordingly, to test the hypothesis whether the higher inflammogenic potency of MWCNT is related to lower-than-unit assemblage density, this means structure, or material-specific intrinsic properties, the concentrations reported by Elder *et al.* (2005) for CB were divided by 10 for MWCNT.

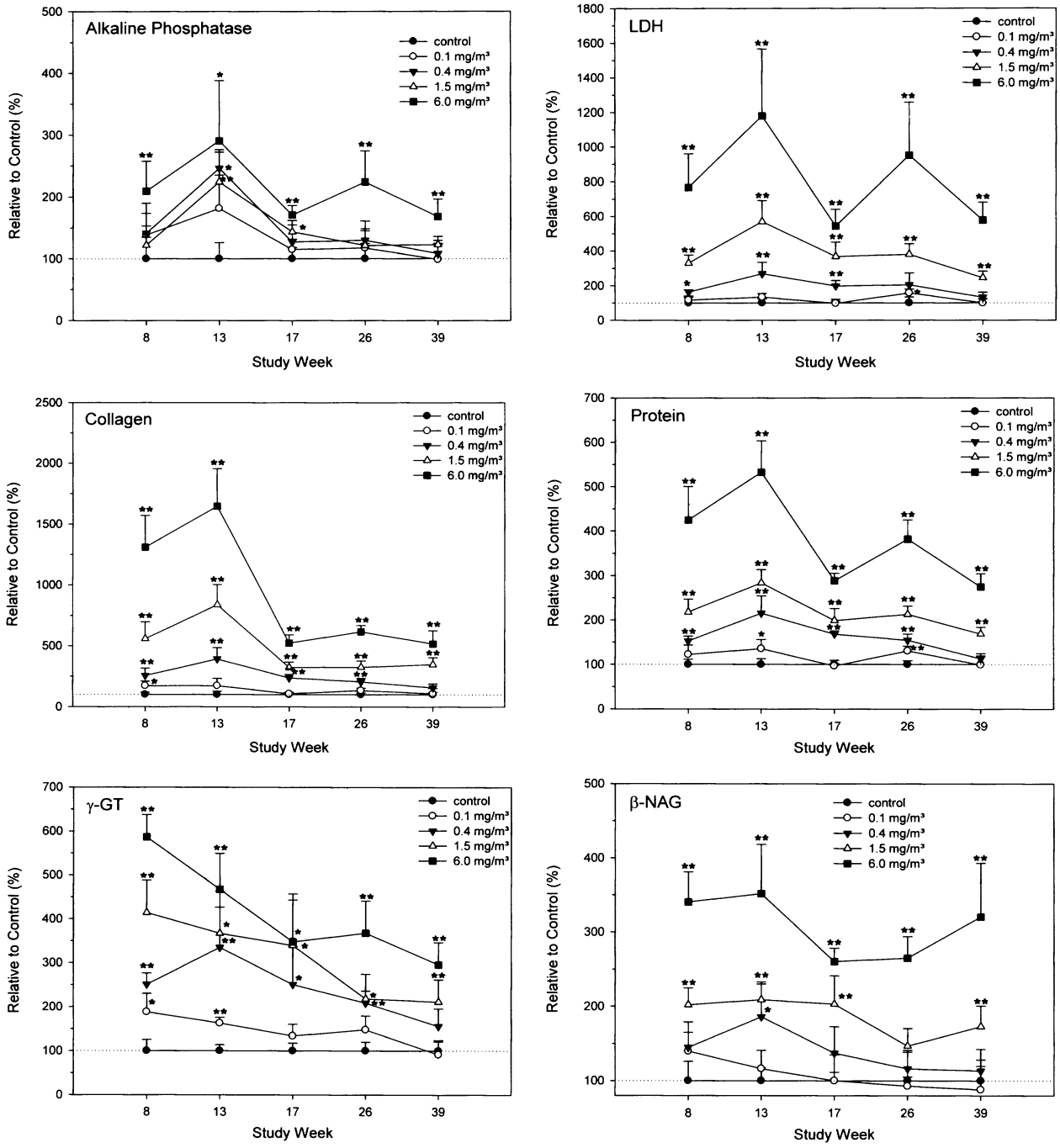

FIG. 9. Time course and concentration dependence of acellular end points in BAL from rats exposed for 8 weeks (interim sacrifice) and 13 weeks (6 h/day, 5 days/week). Data points represent the mean ± SD of six male rats examined on study weeks 13 (postexposure day 1), 17, 26, and 39. Asterisks denote statistical significance to the time-matched control (*$p < 0.05$, **$p < 0.01$).

In regard to the "intrinsic properties" of MWCNT, one needs to appreciate that the high specific surface area and activity of both CB and MWCNT (≈250 m^2/g) promote the adsorption of peptides/proteins contained in the alveolar lining fluid (Dutta *et al.*, 2007; Ehrenberg *et al.*, 2009; Salvador-Morales *et al.*, 2008; Schleh and Hohlfeld, 2009). Hence, recurrent inhalation exposure may both "titrate out" surfactant components, and the resultant opsonization might modulate their attractiveness to alveolar macrophages. Therefore, as long as homeostatically controlled compensation prevails, not all ensuing "changes" are necessarily adverse.

In regard to MWCNT, many material-related and mode-of-testing–related variables have to be accounted for. Among

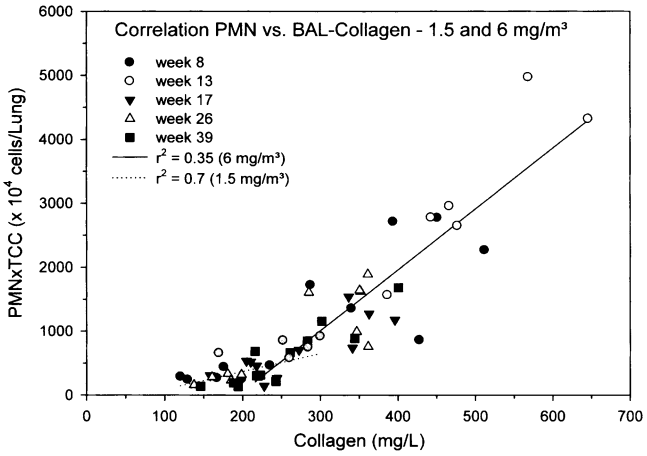

FIG. 10. Correlation of soluble collagen and PMN in BAL from individual rats exposed at 1.5 (doted regression line) and 6 mg/m^3 (solid regression line) and sacrificed during weeks 8, 13, 17, 26, and 39.

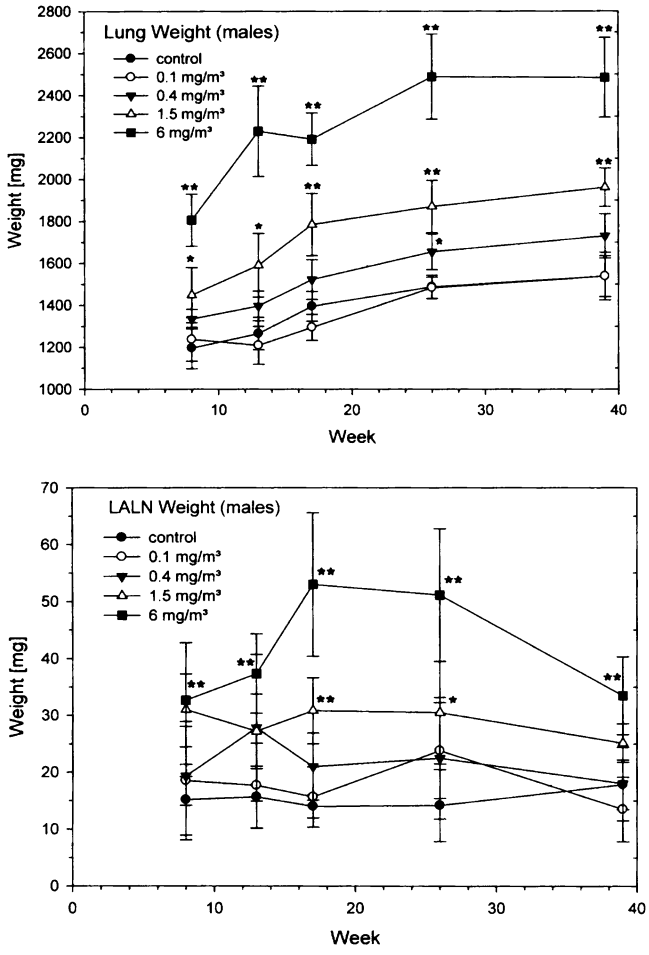

FIG. 11. Lung and LALN weights (wet organ weights) from rats exposed for 8 weeks (interim sacrifice) and 13 weeks (6 h/day, 5 days/week). Data points represent the mean ± SD of six male rats examined on study weeks 13 (postexposure day 1), 17, 26, and 39. Asterisks denote statistical significance to the time-matched control (*$p < 0.05$, **$p < 0.01$).

others, these include nanotube diameter and length, surface functionalization, and the various types of adhesion forces acting between tube surfaces. These variables may determine whether MWCNT are present as isolated fibers or as self-assembled, intertwined, and coil-like structures (assemblages). Electrostatic forces may, however, also be generated as soon as the dispersion, that is, the separation of solid particle surfaces, has taken place. Uncontrolled electrostatic charging of MWCNT cannot only lead to their immediate reagglomeration but it may also generate adhesion forces that increase their deposition within the airways of the upper respiratory tract, especially the larynx. The methods utilized in this study prevented such uncontrolled charging to occur by excluding any one-directional grinding or excessive brushing of the solid test material. Laryngeal findings occurred in studies that did not observe these prerequisites (Ma-Hock *et al.*, 2009). It might be argued that the low humidity used in this study promotes particle reagglomeration. However, this trade-off is made based on previous experience, which showed that high-humidity feed air into dust-generating systems may increase the day-to-day fluctuation in exposure concentrations and may also confound nonspecific mass analyses of very low concentrations due to humidity adsorption in sampling matrices (filter, TEOM). Repeated rat inhalation studies using either low- or high-humidity atmospheres did not reveal any humidity-specific differences (Pauluhn and Mohr, 1999).

The MWCNT evaluated in this study have a spherical to oval shape with a somewhat frayed surface following dispersion into inhalation chambers. The void space of low-density MWCNT within alveolar macrophages may produce a greater displacement volume in alveolar macrophages than high-density solid particles (Brown *et al.*, 2005; Morrow 1988, 1992; Oberdörster *et al.*, 1992). Accordingly, assemblages of MWCNT may trigger pulmonary overload-related cascades of events at lower mass-based exposure levels than the high-density poorly soluble particles studied in the past. In this context, it is important to recognize that the specific density of assemblages/agglomerates interrelates the particle mass metric with the void space–dependent volumetric.

Measurements of the aerodynamic and physical characteristics of MWCNT provide evidence that the aerosolization of this test material generated particles of adequate respirability to rats and that the applied procedures did not alter the physical properties of this test material to any appreciable extent. Co concentrations (constituent impurity related to the catalyst Co used in the production of these types of MWCNT) and N_2-BETs were identical in the starting and micronized materials, which substantiate that artifactual substructures were not produced by the procedures applied. The assemblage structures present in exposure atmospheres and those retained in the lung, as quantified in digested BAL cells, were essentially identical. Fiber-like structures were found neither in exposure atmospheres nor in digested BAL cells. Time-course analysis of BAL

TABLE 3
Pulmonary Histopathology Severity Scores[a] of Most Salient Histopathology Findings in Male Rats following Subchronic MWCNT Exposure

	Concentration (mg/m^3)				
	0	0.1	0.4	1.5	6
Particle-laden macrophages in BALT					
Week 8	0	0	0.5	1.0**	0.8**
Week 13	0	0.3	0.4*	0.6**	0.9**
Week 17	0	0.5	0.7*	1.0**	1.0**
Week 26	0	0.2	0.5	1.0**	1.2**
Week 39	0	0.3	0.2	0.8*	1.0**
Alveolus, interstitial (septal) thickening					
Week 8	0	0	0	0	0
Week 13	0	0	0.9**	1.3**	2.0**
Week 17	0	0.3	1.0**	2.0**	2.2**
Week 26	0	0.2	1.0**	1.8**	2.2**
Week 39	0	0	1.0**	2.0**	2.7**
Pleural thickening					
Week 8	0	0	0	0	0
Week 13	0.1	0	0	0.5	1.0**
Week 17	0	0	0	0.2	0.7*
Week 26	0	0	0.2	0.5	1.0*
Week 39	0.3	0	0.3	0.7	1.0*
Hypercellularity BAJ					
Week 8	0	0	0.3	1.5**	2.0**
Week 13	0	0	0.9**	1.7**	2.1**
Week 17	0	0	1.0**	2.0**	2.3**
Week 26	0	0	1.0**	1.7**	2.0**
Week 39	0	0	0.2	1.7**	1.3**
Terminal bronchiole/alveolus, focal-widespread[a] inflammatory cell influx					
Week 8	0	0	0	0	0–0[b]
Week 13	0.1	0	0.7**	1.6**	0–2.8**
Week 17	0	0.2	0	0.3	1.3**–0
Week 26	0.2	0.2	0.2	0.8	0.8–0.3
Week 39	0.2	0.3	0.7	1.0**	2.0**–0.2
Terminal bronchiole/alveolus, hyperplasia					
Week 8	0	0	0	0	0
Week 13	0	0	0	0	0
Week 17	0	0	0	0	0.2
Week 26	0	0	0	0	0.8
Week 39	0	0	0	0	1.5**
Terminal bronchiole/peribronchiolar, focally increased collagen staining					
Week 8	0	0	0	1.0**	1.0**
Week 13	0	0	1.0**	0	0
Week 17	0	0	1.0**	0	0
Week 26	0	0.2	0.8**	0	0
Week 39	0	0	1.2**	0	0
Terminal bronchiole/peribronchiolar, increased collagen staining					
Week 8	0	0	0	0	0
Week 13	0	0	0	1.6**	2.8**
Week 17	0	0	0	1.5**	1.2**
Week 26	0	0	0.2	1.5**	2.0**
Week 39	0	0	0	2.0**	2.5**

Note. BALT: bronchus-associated lymphatic tissue, BAJ, bronchioloalveolar junction.

[a]Severity scores given to individual animal from a complete pathological examination are 0, not remarkable; 1, minimal; 2, slight/mild; 3, moderate; 4, moderately severe; and 5 severe, based upon relative evaluation of lesions. Severity scores for each animal within a group were added, and an average score per animal was calculated which is shown in the table.

[b]More widespread inflammatory responses occurred at 6 mg/m^3 only. The lavaged lungs of six male rats per group were examined during weeks 8, 17, 26, and 39. The nonlavaged lungs of 10 male rats per group (females not shown) were examined in week 13. Asterisks denote statistical significant differences of incidences to the control (*$p < 0.05$, **$p < 0.01$) using Fisher's Exact Test.

cells harvested at the end of the 3-month exposure and 6-month postexposure periods did not provide experimental evidence of any time-related changes in the characteristics of assemblages retained in alveolar macrophages.

The pulmonary dosimetry of MWCNT is analytically demanding. Hence, the matrix-bound impurities of the catalyst Co were used as marker of exposure. Time-course–related changes in lung burdens were small both during the exposure period (weeks 8–13) and postexposure period (weeks 13–39). In contrast, Co burdens in LALNs were clearly dependent on the cumulative exposure dose. Thus, the time-course–related changes in pulmonary inflammation, as evidenced by measurements in BAL, and the respective changes in Co lung burdens did not change in concert, which needs further attention in future studies. However, a reasonable match of empirical data and simulated Co lung burdens was achieved based on the constraints and parameterization given in the Materials and methods section (Kinetic Analysis of Co Lung Burdens section). This similarity supports the supposition that MWCNT assemblages were not deposited to any unbalanced extent in the upper airways due to interceptive forces in addition to the inertia-related impaction forces. Interestingly, the retention halftimes of CB at 7 mg/m^3 and MWCNT at 6 mg/m^3 were $t_{1/2} = 329$ days and $t_{1/2} = 375$ days, respectively, were remarkably close at about six times the overload threshold (Pauluhn, 2009a). This similarity supports the conclusions of this study, namely, that MWCNT show properties somewhat similar to those described for poorly soluble higher-than-unit density particles (ILSI, 2000). However, overload-related inflammation may occur much earlier as detailed below. In regard to toxicological significance, the retention kinetics at high exposure levels makes it unlikely that a postexposure period as "short" as 6 months ($\approx 0.5\ t_{1/2}$) is suitable to reveal any appreciable reversibility in this bioassay.

Morrow (1988, 1994) suggested that a rats' macrophage-mediated clearance is impaired at a volumetric loading of 60 cubic microns per alveolar macrophage and that macrophage stasis occurred at a loading of 600 μm^3. These volumes represent approximately 6 and 60% of the alveolar

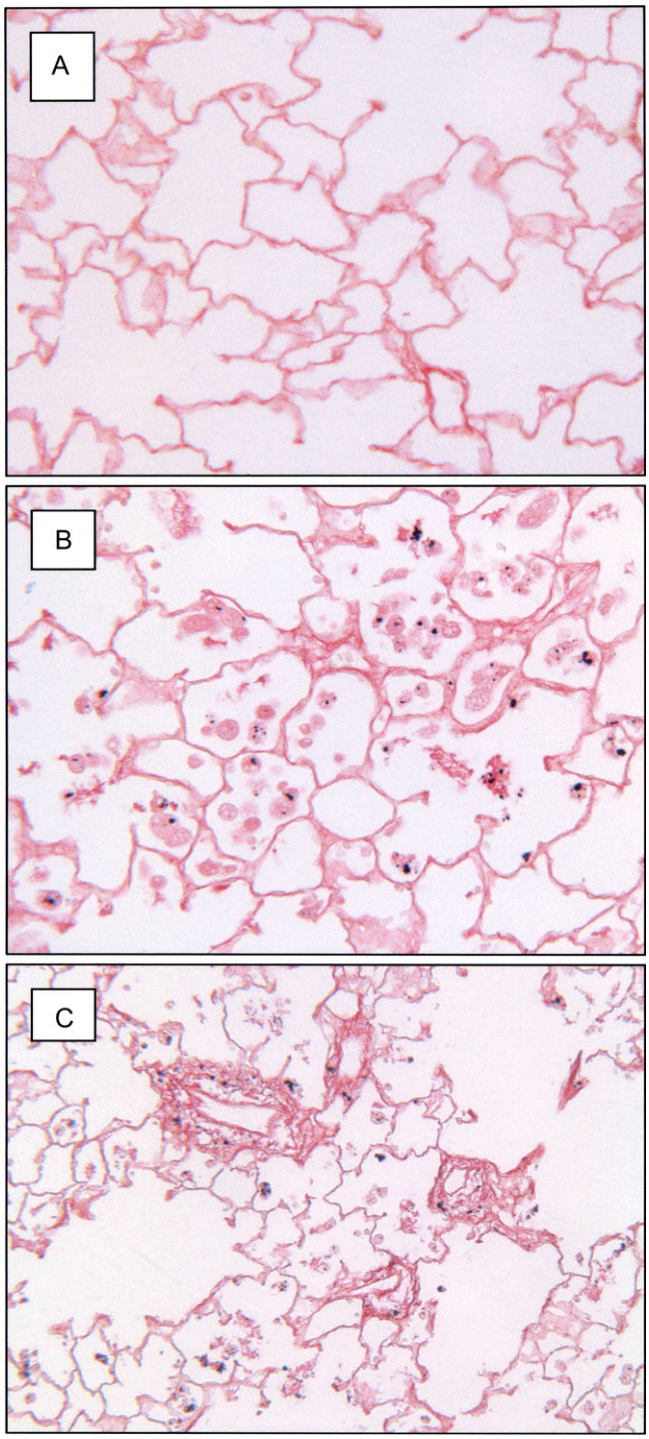

FIG. 12. Sirius red–stained lung sections (week 13, nonlavaged lungs, magnification: ×25) from rats exposed to air (A) and at 6 mg/m^3 (B and C). Focally increased collagen staining was adjacent to deposited particles, particle-laden macrophages, and inflammatory infiltrates.

macrophage's displacement volume and correspond to the volume loadings of 1000 and 10,000 nl/g lung, respectively (Brown *et al.*, 2005). Clearance rates do not differ from control at the volume loading of 100 nl/g lung or 6 cubic microns per alveolar macrophage (Morrow, 1994). A loading of 1400 nl/g lung can be inferred as doubling of clearance halftimes (Oberdörster, 1995). Within the macrophage, the occupying volume from nonuniform, light-density MWCNT may be appreciably higher than the idealized volume of the MWCNT themselves. When calculating the cumulative lung burden of deposited MWCNT using a density of MWCNT assemblages in the range of 0.1–0.3 g × cm^{-3} (see Table 1), then the yields of volumetric lung burdens are in the range of 107–325, 466–1413, 1192–3917, and 3961–12,002 nl/g lung at 0.1, 0.4, 1.5, and 6 mg/m^3, respectively (corrected for void space volume which is 1.43 times greater than the volume of the MWCNT themselves; Brown *et al.*, 2005). Interestingly, in regard to estimates of lung overload, the results from mass-based kinetic analyses and cumulative volumetric lung burdens based on respirable mass converge into similar conclusions. Therefore, it appears that the findings of this study are fairly consistent with the work of Morrow (1988, 1994) and Brown *et al.* (2005) as well as the deliberations from an ILSI conference addressing the interrelationship of lung overload and inflammation (ILSI, 2000). This means, in concert with the hypothesis of this study, the concentrations of 0.1 and 0.4 mg/m^3 MWCNT examined are covering the range of minimal to moderate lung overload, whereas impaired clearance to complete stasis may have happened at 1.5 and 6 mg/m^3.

Consequently, the comparison CB and MWCNT supports the hypothesis of this study, namely, that the etiopathology of both poorly soluble particles is triggered by a similar cascade of events. However, the observed differences in toxic potencies appear to be linked to their markedly different specific densities of agglomerates or assemblages. The resultant higher displacement volumes in alveolar macrophages may then lead to an earlier attainment of a lung overload-related inhibition of clearance and disproportionally increased pulmonary inflammation.

Pulmonary toxicity as characterized by histopathology occurred in a concentration-dependent and sustained manner beginning at 0.4 mg/m^3 (Table 3). Slight to moderate inflammation, focally also with granulomatous appearance, was only apparent in rats exposed at 6 mg/m^3. Evidence of cytotoxicity (LDH) and changes considered to be related to dysfunctional surfactant (BAL cells with foamy appearance) predominated at 1.5 and 6 mg/m^3. In regard to concentration and time response, PMNs and collagen were the most consistent and sensitive end points in BAL (Figs. 8 and 9) to probe for MWCNT-induced effects. Their high correlation (Fig. 10) supports the notion that the soluble collagen in BAL is caused by extravasation rather than localized tissue processes, as already hypothesized by previous studies (Ellinger and Pauluhn, 2010). While there was only mild attenuation in the severity of the inflammatory response probed by BAL at 1.5 and 6 mg/m^3 during the 6-month postexposure period, attenuation of elevations occurred at 0.4 mg/m^3. Borderline, although significant, elevations of γ-GT and protein occurred already at 0.1 mg/m^3. However, due the absence of any other effect suggestive of pulmonary toxicity, the isolated and transitional changes of protein and γ-GT appear to be

consistent with an adaptive rather than any adverse causality, possibly due to an affected surfactant homeostasis.

Histopathology demonstrated a complementary picture to BAL analyses. Likewise, the histopathology findings were consistent with a cumulative exposure dose–related alveolitis and associated hallmarks, such as septal and pleural thickening at 1.5 and 6 mg/m^3. The mammalian lung has a network of lymphatic plexi within the connective tissue of the visceral pleura and tissues surrounding the airways, arteries, and veins (Lauweryns and Baert, 1977). The time course and concentration dependence of elevated Co burdens in LALNs (Fig. 7), including their weights (Fig. 11), as well as the histological evidence of increased pleural inflammation (Table 3), appear to demonstrate a relationship to alveolitis.

After the 13-week exposure period, inflammatory changes occurred both in the more distal nasal cavities and in the lower respiratory tract at 0.4 mg/m^3 and above. The localized changes observed appear to reflect the localized pattern of deposition of MWCNT. Yet, nonspecific responses to localized particle overload in the nasal cavities of rats have not received increased attention in repeated exposure inhalation studies with poorly soluble particles. Of note is that similar findings in the nasal cavities of rats subchronically exposed to MWCNT were also found by other authors (Ma-Hock *et al.*, 2009). This appears to support an etiopathological sequence of events dependent on the localized exhaustion of compensatory mechanisms and ensuing changes that make this location often more resistant to such stresses.

In summary, the analysis of time-course changes of Co in lung tissue provided matching evidence of external exposure concentrations and the retained cumulative lung dose. Consistent with the hypothesis of study, the clearance of the less-than-unit density assemblages of MWCNT was somewhat delayed at the lower exposure concentrations while a marked inhibition of clearance was apparent at 1.5 and 6 mg/m^3. Delayed particle clearance and associated sustained pulmonary inflammation are typical findings in rats exposed under conditions attaining lung overload (Brown *et al.*, 2005; Elder *et al.*, 2005; ILSI, 2000; Morrow, 1988; Oberdörster, 1995). Under such conditions, extensive alveolitis occurs, which also may deteriorate the alveolar barrier function. Thus, increased particle translocation to the draining lymph nodes of the lung appears to be a result of inflammation severity and is not necessarily any nanoparticle property. This study supports the supposition that MWCNT do not disaggregate in the alveolus to produce nanoparticles or nanofibers. In regard to the intensity and attenuation of effects during a 6-month postexposure period, 0.4 mg/m^3 represents the transitional range where overloading-related mechanisms start to become operative. Collective evidence supports the conclusion that 0.1 mg/m^3 constitutes the no-observed-adverse-effect-level of this study based on nasal and pulmonary inflammatory responses, this means at the sites where predominant particle deposition occurs. Suffice it to say, due to the variability of engineered CNT, as already pointed out in the Introduction, the results obtained with this particular MWCNT (Baytubes) may not necessarily apply to nanotubes with differing physicochemical characteristics.

ACKNOWLEDGMENTS

The author thanks Dr I. Loof for determinations in lung lavage, Dr Schweer (Currenta) for determinations of Co in tissues, Dr M. Voetz (Bayer Technology Services) for data related to the characterization of the test substance, and Prof Dr M. Rosenbruch for histopathology data. SEM/EDX analyses on digested cytospins were performed by Prof Dr M. Wiemann, IBE R&D GmbH, Institute for Lung Health, Marl, Germany. Conflict of interest: The investigation of this proprietary product of Bayer Material Science took place during the normal course of employment with Bayer Schering Pharma. The interpretation of study is that of the author and not the employer.

REFERENCES

Anjilvel, S., and Asgharian, B. (1995). A multiple-path model of particle deposition in the rat lung. *Fundam. Appl. Toxicol.* **28,** 41–50.

Baron, P. A., Deye, G. J., Chen, B. T., Schwegler-Berry, D. E., Shvedova, A. A., and Castranova, V. (2008). Aerosolization of single-walled carbon nanotubes for an inhalation study. *Inhal. Toxicol.* **20,** 751–760.

Bermudez, E., Mangum, J. B., Asgharian, B., Wong, B. A., Revery, E. E., Janszen, D. B., Hext, P. M., Warheit, D. B., and Everitt, J. I. (2002). Long-term pulmonary responses of three laboratory rodent species to subchronic inhalation of pigment-grade titanium dioxide particles. *Toxicol. Sci.* **70,** 86–97.

Bermudez, E., Mangum, J. B., Wong, B. A., Asgharian, B., Hext, P. M., Warheit, D. B., and Everitt, J. I. (2004). Pulmonary responses of mice, rats, and hamsters to subchronic inhalation of ultrafine titanium dioxide particles. *Toxicol. Sci.* **77,** 347–357.

Brain, J. D., and Frank, N. R. (1968a). Recovery of free cells from rat lungs by repeated washings. *J. Appl. Physiol.* **25,** 63–69.

Brain, J. D., and Frank, N. R. (1968b). The relation of age to the numbers of lung free cells, lung weight, and body weight in rats. *J. Gerontol.* **23,** 58–62.

Brown, J. S., Wilson, W. E., and Grant, L. D. (2005). Dosimetric comparisons of particle deposition and retention in rats and humans. *Inhal. Toxicol.* **17,** 355–385.

Brunauer, S., Emmet, P. H., and Teller, E. (1938). Adsorption of gases in multimolecular layers. *J. Am. Chem. Soc.* **60,** 309–318.

Directive 86/609/EEC. (1986). Guideline of the council dated November 24, 1986 on the reconciliation of legal and administrative regulations of the member countries for the protection of animals used for studies and other scientific purposes. *J. Eur. Commun.* Legal Spec. L358 **29,** 1–28.

Duffin, R., Mills, N. L., and Donaldson, K. (2007). Nanoparticles-a thoracic toxicology perspective. *Yonsei Med. J.* **48,** 561–572.

Dutta, D., Sundaram, S. K., Teeguarden, J. G., Riley, B. J., Fifield, L. S., Jacobs, J. M., Addleman, S. R., Kaysen, G. A., Moudgil, B. M., and Weber, T. J. (2007). Adsorbed proteins influence the biological activity and molecular targeting of nanomaterials. *Toxicol. Sci.* **100,** 303–315.

Ehrenberg, M. S., Friedman, A. E., Finkelstein, J. N., Obderdörster, G., and McGrath, J. I. (2009). The influence of protein adsorption on nanoparticle association with cultured endothelial cells. *Biomaterials* **30,** 603–610.

Elder, A., Gelein, R., Finkelstein, J. N., Driscoll, K. E., Harkema, J., and Oberdörster, G. (2005). Effects of subchronically inhaled carbon black in three species. I. Retention kinetics, lung inflammation, and histopathology. *Toxicol. Sci.* **88,** 614–629.

Ellinger-Ziegelbauer, H., and Pauluhn, J. (2010). Pulmonary toxicity of multi-walled carbon nanotubes (Baytubes) relative to a-quartz following a single 6 hour inhalation exposure of rats and a 3 months postexposure period. *Toxicology*. Advance Access published on October 14, 2009; doi:10.1016/j.tox.2009.10.007.

Fenoglio, I., Greco, G., Tomatis, M., Muller, J., Raymundo-Piñero, E., Béguin, F., Fonseca, A., Nagy, J. B., Lison, D., and snd Fubini, B. (2008). Structural defects play a major role in the acute lung toxicity of multiwall carbon nanotubes: Physicochemical aspects. *Chem. Res. Toxicol* **21,** 1690–1697.

International Life Science Institute (ILSI) (2000). The relevance of the rat lung response to particle overload for human risk assessment: A workshop consensus report—ILSI Risk Science Institute workshop participants. *Inhal. Toxicol.* **12,** 1–17.

Kaufmann, W., Bader, R., Ernst, H., Harada, T., Hardisty, J., Kittel, B., Kolling, A., Pino, M., Renne, R., Rittinghausen, S., *et al.* (2009). "Larynx squamous metaplasia": A re-consideration of morphology and diagnostic approaches in rodent studies and its relevance for human risk assessment. *Exp. Toxicol. Pathol.* Advance Access published on March 12, 2009; doi:10.1016/j.etp.2009.01.001.

Klobes, P., Meyer, K., and Munro, R. G. (2006). In *Porosity and Specific Surface Area Measurements for Solid Materials. National Institute of Standards and Technology (NIST) Recommended Practice Guide*. Special Publication 960-17. U.S. Department of Commerce, Washington, DC.

Lam, C. W., James, J. T., McCluskey, R., Arepalli, S., and Hunter, R. L. (2006). A review of carbon nanotube toxicity and assessment of potential occupational and environmental health risks. *Crit. Rev. Toxicol.* **36,** 189–217.

Lauweryns, J. M., and Baert, J. H. (1977). Alveolar clearance and the role of the pulmonary lymphatics. *Am. Rev. Respir. Dis.* **115,** 625–683.

Ma-Hock, L., Treumann, S., Strauss, V., Brill, S., Luizi, F., Mertler, M., Wiench, K., Gamer, A. O., van Ravenzwaay, B., and Landsiedel, R. (2009). Inhalation toxicity of multi-wall carbon nanotubes in rats exposed for 3 months. *Toxicol. Sci.* Advance Access published on July 7, 2009; doi:10.1093/toxsci/kfp146.

Mauderly, J. L. (1986). Respiration of F344 rats in nose-only inhalation exposure tubes. *J. Appl. Toxicol.* **6,** 25–30.

Maynard, A. D. (2007). Nanotechnology: The next big thing, or much ado about nothing? *Ann. Occup. Hyg.* **51,** 1–12.

Morrow, P. E. (1988). Possible mechanisms to explain dust overloading of the lungs. *Fundam. Appl. Toxicol.* **10,** 369–384.

Morrow, P. E. (1992). Dust overloading in the lungs. *Toxicol. Appl. Toxicol.* **113,** 1–12.

Morrow, P. E. (1994). Mechanisms and significance of "particle overload". In *Toxic and Carcinogenic Effects of Solid Particles in the Respiratory Tract: Proceedings of the 4th International Inhalation Symposium*; March 1993, Hannover, Germany, pp. 17–25. Washington, DC: International Life Sciences Institute Press.

Muller, J., Delos, M., Panin, N., Rabolli, V., Huaux, F., and Lison, D. (2009). Absence of carcinogenic response to multi-wall carbon nanotubes in a 2-year bioassay in the peritoneal cavity of the rat. *Toxicol. Sci.* **110,** 442–448.

Muller, J., Huaux, F., Fonseca, A., Nagy, J. B., Moreau, N., Delos, M., Raymundo-Piñero, E., Béguin, F., Kirsch-Volders, M., Fenoglio, I., *et al.* (2008). Structural defects play a major role in the acute lung toxicity of multiwall carbon nanotubes: Toxicological aspects. *Chem. Res. Toxicol.* **21,** 1698–1705.

National Institute for Public Health and the Environment (RIVM). (2002). *Multiple Path Particle Dosimetry Model (MPPD2 v. 1.0): A Model for Human and Rat Airway Particle Dosimetry*. Bilthoven, The Netherlands. RIVA Report 650010030.

National Research Council (NRC). (2007). *Toxicity Testing in the 21st Century. A Vision and a Strategy*. The National Academies Press, Washington, DC.

Oberdörster, G. (1995). Lung particle overload: Implications for occupational exposures to particles. *Regul. Toxicol. Pharmacol.* **27,** 123–135.

Oberdörster, G. (2002). Toxicology of ultrafine particles: In vivo studies. *Philos. Trans. R. Soc. Lond. B Biol. Sci.* **A358,** 2719–2740.

Oberdörster, G., Ferin, J., and Morrow, P. E. (1992). Volumetric loading of alveolar macrophages (AM): A possible basis for diminished AM-mediated particle clearance. *Exp. Lung Res.* **18,** 87–104.

Oberdörster, G., Oberdörster, E., and Oberdörster, J. (2005). Nanotoxicology: An emerging discipline evolving from studies of ultrafine particles. *Environ. Health Perspect.* **113,** 823–839.

Oberdörster, G., Oberdörster, E., and Oberdörster, J. (2007). Concepts of nanoparticle dose metric and response metric. *Environ. Health Perspect.* **115,** A290.

Organisation for Co-Operation and Development (OECD). (2008). *Guideline for the Testing of Chemicals. Draft Proposal for a Revised Guideline 413: Subchronic Inhalation Toxicity: 90-Day Study*. Environment Directorate, Organization for Economic Cooperation and Development, Paris, France. Available at: http://www.oecd.org/dataoecd/62/28/41460877.pdf. Accessed September 30, 2008.

OECD. (2009). *Environment, Health and Safety Publications, Series on Testing and Assessment No. 39: Guidance Document for Acute Inhalation Toxicity Testing, ENV/JM/MONO 28*. pp. 71, Paris, France. Available at: http://www.oecd.org/document/30/0,3343,en_2649_34377_1916638_1_1_1_1,00.html. Accessed July 21, 2009.

Pauluhn, J. (1994). Validation of an improved nose-only exposure system for rodents. *J. Appl. Toxicol.* **13,** 55–62.

Pauluhn, J. (2005). Retrospective analysis of acute inhalation toxicity studies: Comparison of actual concentrations obtained by filter and cascade impactor analyses. *Regul. Toxicol. Pharmacol.* **42,** 236–244.

Pauluhn, J., and Mohr, U. (1999). Repeated 4-week inhalation exposure of rats: Effect of low-, intermediate, and high-humidity chamber atmospheres. *Exp. Toxicol. Pathol.* **51,** 178–187.

Pauluhn, J. (2009a). Comparative pulmonary response to inhaled nanostructures: Considerations on test design and endpoints. *Inhal. Toxicol.* **21**(S1), 40–54.

Pauluhn, J. (2009b). Pulmonary toxicity and fate of agglomerated 10 and 40 nm aluminum oxyhydroxides following 4-week inhalation exposure of rats: Toxic effects are determined by agglomerated, not primary particle size. *Toxicol. Sci.* **109,** 152–167.

Pauluhn, J. (2010). Multi-walled carbon nanotubes (baytubes): approach for derivation of occupational exposure limit. *Regul. Toxicol. Pharmacol.* (Forthcoming).

Pauluhn, J., and Thiel, A. (2007). A simple approach to validation of directed-flow nose-only inhalation chambers. *J. Appl. Toxicol.* **27,** 160–167.

Poland, C. A., Duffin, R., Kinloch, I., Maynard, A., Wallace, W. A., Seaton, A., Stone, V., Brown, S., Macnee, W., and Donaldson, K. (2008). Carbon nanotubes introduced into the abdominal cavity of mice show asbestos-like pathogenicity in a pilot study. *Nat. Nanotechnol.* **3,** 423–428.

Salvador-Morales, C., Basiuk, E. V., Basiuk, V. A., Green, M. L., and Sim, R. B. (2008). Effects of covalent functionalization on the biocompatibility characteristics of multi-walled carbon nanotubes. *J. Nanosci. Nanotechnol.* **8,** 2347–2356.

Schleh, C., and Hohlfeld, J. M. (2009). Interaction of nanoparticles with the pulmonary surfactant system. *Inhal. Toxicol.* **21**(S1), 97–103.

Shvedova, A. A., Kisin, E. R., Porter, D., Schulte, P., Kagan, V. E., Fadeel, B., and Castranova, V. (2009). Mechanisms of pulmonary toxicity and medical applications of carbon nanotubes: Two faces of Janus? *Pharmacol. Ther.* **121,** 192–204.

Takagi, A., Hirose, A., Nishimura, T., Fukumori, N., Ogata, A., Ohashi, N., Kitajima, S., and Kanno, J. (2008). Induction of mesothelioma in p53+/- mouse by intraperitoneal application of multi-wall carbon nanotube. *J. Toxicol. Sci.* **33,** 105–116.

Walker, N. J., and Bucher, J. R. (25 May 2009). A 21st century paradigm for evaluating the health hazards of nanoscale materials? *Toxicol. Sci.* **110,** 251–254.

Warheit, B. D. (2008). How meaningful are the results of nanotoxicology studies in the absence of adequate material characterization? *Toxicol. Sci.* **101,** 183–185.

Warheit, D. B., Laurence, B. R., Reed, K. L., Roach, D. H., Reynolds, G. A., and Webb, T. R. (2004). Comparative pulmonary toxicity assessment of single-wall carbon nanotubes in rats. *Toxicol. Sci.* **77,** 117–125.

Willeke, K., and Baron, P. A. (1993). In *Aerosol Measurement—Principles, Techniques, and Applications*. Van Nostrand Reinhold, New York.

Young, J. T. (1981). Histopathologic examination of the rat nasal cavity. *Fundam. Appl. Toxicol.* **1,** 309–312.

Zbib, A. A., Mesarovic, S. D.j., Lilleodden, E. T., McClain, D., Jiao, J., and Bahr, D. F. (2008). The coordinated buckling of carbon nanotubes turfs under uniform compression. *Nanotechnology* **19,** 1–7.